Preparation and physiochemical analysis of novel ciprofloxacin / dicarboxylic acid salts

Journal of Pharmaceutical Sciences 112 (2023) 195–203

Contents lists available at ScienceDirect

Journal of Pharmaceutical Sciences

journal homepage: www.jpharmsci.org

Pharmaceutics, Drug Delivery and Pharmaceutical Technology

Preparation and Physiochemical Analysis of Novel Ciprofloxacin / Dicarboxylic Acid Salts

Thomas Hibbard[a], Bildad Nyambura[b], Peter Scholes[b], Mihaela Totolici[b], Kenneth Shankland[a,*], Hisham Al-Obaidi[a,*]

[a] School of Pharmacy, University of Reading, Reading, RG6 6AD, UK
[b] Quotient Sciences, 5 Boulton Road, Reading, RG2 0NH, UK

ARTICLE INFO

Article history:
Received 19 April 2022
Revised 27 July 2022
Accepted 5 August 2022
Available online 8 August 2022

Keywords:
Mechanochemical activation
Crystalline salts
Ciprofloxacin
Single crystal
Thermal analysis
Solubility

ABSTRACT

The crystal structures of four novel dicarboxylic acid salts of ciprofloxacin (CFX) with modified physicochemical properties, prepared by mechanochemical synthesis and solvent crystallization, are reported. A series of dicarboxylic acids of increasing molecular weight was chosen, predicted to interact via a carboxylic acid:secondary amine synthon. These were succinic (SA), glutaric (GA), adipic (AA) and pimelic (PA) acids (4, 5, 6, 7 carbon atoms respectively). Characterized by single crystal and powder X-ray diffraction, Fourier-Transform Infrared Spectroscopy, thermogravimetric analysis, differential scanning calorimetry, scanning electron microscopy and aqueous solubility measurements, these salts showed distinct physicochemical properties relative to ciprofloxacin base. Searches of the Cambridge Structural Database (CSD) confirmed CFX-SA, CFX-GA, CFX-AA and CFX-PA to be novel crystal structures. Furthermore, the GA salt has substantially higher solubility than the widely available hydrochloride monohydrate salt (CFX-HCl·H_2O). CFX-SA, CFX-GA and CFX-AA showed minimum inhibitory concentration (MIC) of 0.008 g/L and CFX-PA showed MIC of 0.004 g/L. The prepared CFX salts retained antibacterial activity exhibiting equivalent antimicrobial activity to CFX-HCl·H_2O. These salts have positive implications for increasing the application of CFX beyond conventional oral formulations and highlight mechanochemical activation as suitable production method.

Introduction

Aqueous solubility of active pharmaceutical ingredients (APIs) can be improved through the discovery of new solid forms. Common examples of different solid forms used are salts, polymorphs, amorphous and coamorphous forms, cocrystals, solvates and hydrates; these are the subject of several extensive reviews and studies.[1-7] In each of these cases, the same API can exhibit different physiochemical properties without change to the chemical structure.[8-10] Novel solid forms have a variety of applications[11,12] in oral and pulmonary drug delivery, and cocrystals, organic salts and inorganic salts showing a variety of physicochemical properties have previously been reported.[13-17]

Fluoroquinolone antibiotics, such as ciprofloxacin (CFX), have been the subject of a great deal of solid-state research due to their poor aqueous solubility.[18,19] CFX is classified as class IV drug exhibiting poor aqueous solubility and permeability limiting its absorption and bioavailability.[20] Recent application of CFX to target lung infections has showed significant improvement when delivered as dry powder directly to the lungs.[21] Nevertheless, the problem of poor solubility remains a challenge and a problem that requires crystal engineering approach. Salt formation is the most well-established among other methods and has brought many APIs to market, usually through increasing API solubility.[22,23] Although the hydrocholoride salt is often the preferred candidate, it is also associated with increased hygroscopicity leading to problems with manufacturing.[24,25] This can have a negative impact on applications in drug delivery to the lungs when dry powders are desired. Whilst there has been diverse research on inorganic counterions, the use of organic counterions remains relatively limited.

In this work, a series of four potential dicarboxylic acid counterions with increasing molecular weight was selected for study. Similar molecules have also been investigated for their synergistic antibacterial, antibiofilm effects. For example, Bahamondez-Canas et al. showed that succinic acid stimulated degeneration of biofilm, allowing enhanced killing of *P. aeruginosa*.[26,27] Selecting a series of counterions with increasing carbon chain length allows for a comparison between counterions and final product physicochemical properties.

* Corresponding authors.
E-mail addresses: k.shankland@reading.ac.uk (K. Shankland), h.al-obaidi@reading.ac.uk (H. Al-Obaidi).

https://doi.org/10.1016/j.xphs.2022.08.008

Of the counterions selected, only hydrated forms of ciprofloxacin: succinic acid and ciprofloxacin:adipic acid have previously been reported.[13,28] Crystal structures for four CFX salts are reported, as are their physicochemical properties, thermal behaviour, aqueous solubility and antimicrobial activity.

Experimental Section

Materials: Ciprofloxacin base, ciprofloxacin hydrochloride monohydrate, succinic acid, glutaric acid, adipic acid and pimelic acid were obtained from Sigma-Aldrich (Dorset, UK). Methanol was obtained from Fisher-Scientific Limited (Leicestershire, UK). All chemicals were used as received.

Methods

Counterion Selection

Compatibility screening of CFX against a bank of coformers was performed using the "Co-crystal design" function of Mercury[29] and this yielded approximately 100 potential matches. A series of dicarboxylic acids of increasing molecular weight was chosen, predicted to interact via a carboxylic acid:secondary amine synthon. These were succinic (SA), glutaric (GA), adipic (AA) and pimelic (PA) acids (4, 5, 6, 7 carbon atoms respectively). The 2D structure formulas and physicochemical properties of CFX and the counterions are summarised in Fig. 1. The ΔpK_a (pK_a (base) – pK_a (acid)) values are greater than 3 in each case,[30] suggesting salt formation between the acid-base pairs.

Preparation of CFX Salts

Equimolar quantities of CFX and counterion (1:1 molar ratio) were milled using a Retsch MM400 ball mill. A 25 mL vessel was shaken at 30 Hz for 30 mins with two 7.5 mm stainless steel balls and 20 μL of methanol. This approach to multicomponent crystal synthesis was tested successfully on a known theophylline:nicotinamide system.[31] CFX and counterions were also mixed in a MeOH/ACN (1:1 molar ratio) solvent system at 45°C for 4 to 6 hours. The resultant suspensions were filtered through a 0.22 μm syringe filter (Ministart®) and the filtrates left to saturate by solvent evaporation at 25°C. Resultant crystals were harvested for single crystal X-ray diffraction (SC-XRD). CFX and counterions were also dissolved in aqueous solution at 70°C. Resultant solutions were filtered through a 0.22 μm syringe filter (Ministart®) and left to saturate at 25°C. Resulting crystals were harvested for SC-XRD.

Powder X-ray Diffraction (PXRD)

Transmission capillary PXRD data were collected for all powders post-milling, using a Bruker D8 Advance diffractometer equipped with a monochromatic Cu$K\alpha_1$ source. Samples were packed into 0.7 mm borosilicate glass capillaries then scanned in the range 4° to 45° 2θ using a step size of 0.0171° and a count time of 1.4 seconds per step. PXRD patterns were compared to reference data collected from starting materials using the same settings.

Single Crystal X-ray Diffraction (SC-XRD)

Single crystals showing birefringence under polarised light were isolated in Paratone-N oil, then mounted on a suitable crystal mounting loop. Diffraction data at 100K were collected using a Rigaku Synergy diffractometer equipped with a Cu microsource, a HyPix detector and an Oxford Cryosystems Cryostream device. Crystal structures were solved using ShelXT[32] and refined using ShelXL[33] (running as part of the Olex2[34] system) and crosschecked with the Cambridge Structural Database (CSD) database[35] then rendered using Mercury.[36] The positions of hydrogen atoms were determined directly from the observed electron density. Hydrogen atoms attached to carbons were treated with a riding ('AFIX') model, whilst hydrogen atoms attached to O or N atoms were allowed to refine freely, ensuring that the co-crystal or salt nature of the materials was directly determined.

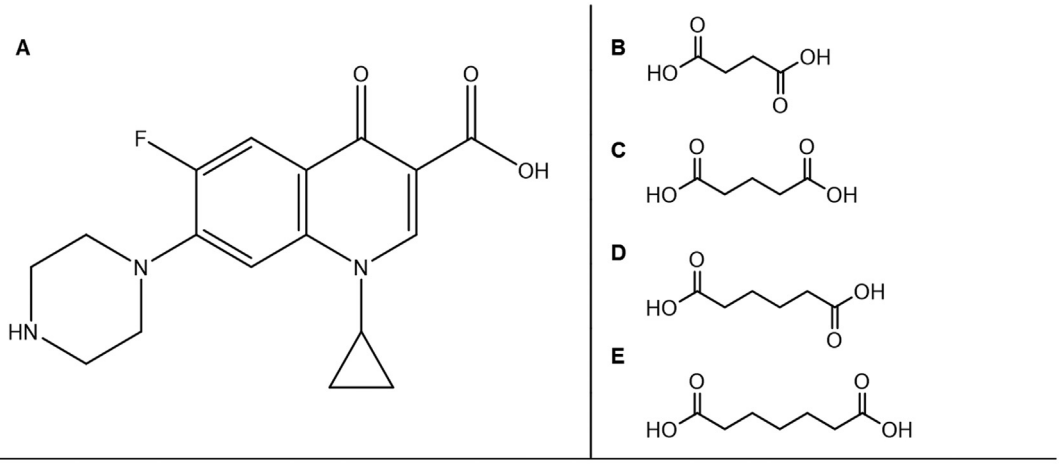

	MWt / gmol^{-1}	MPt / °C	log*P*	pK_a	Water Solubility / mgml^{-1}
Succinic Acid (B)	118.09	188	-0.59	4.21	83.2
Glutaric Acid (C)	132.11	96.9	-0.29	4.34	1600
Adipic Acid (D)	146.14	153.2	0.08	4.44	30.8
Pimelic Acid (E)	160.17	106	0.61	4.51	50
Ciprofloxacin Base (A)	331.35	259	0.28	8.74	1.35

Fig. 1. The structures of ciprofloxacin base and the potential counterions used in this work. Key known physiochemical properties are listed.

Fourier-Transform Infrared Spectroscopy (FTIR)

FTIR spectra were collected using a Perkin-Elmer 100 FTIR Spectrometer equipped with a diamond attenuated total reflectance (ATR) accessory (Shelton, Connecticut, USA). 16 scans were made, with transmission recorded over the range 650–4000 cm^{-1} with a resolution of 4 cm^{-1}.

Thermal Analysis

Melting point analysis was performed for all samples using a TA-Q2000 Differential Scanning Calorimetry (DSC) instrument (TA instruments, New Castle, USA). Samples were hermetically sealed in an aluminium pan and allowed to equilibrate at 30°C before heating at 10°C/min to 280°C in an N_2 atmosphere. Pierced lids were used to avoid issues relating to pressure build up during heating. Thermogravimetric Analysis (TGA) using TA-TGA Q50 instrument (New Castle, USA) was performed by weighing approximately 5-10mg of the samples and heated from ambient temperature at a heating rate of 10°C/min. TA Universal Analysis software was used to describe thermal events and to calculate melting points using onset temperature.

Saturation Solubility Measurement

Excess solid was added to 1 mL of phosphate buffers (0.1M and 0.2M, pH 6.8) and mixed at 25°C (± 1°C) using rotary mixer for 72 hours. Supernatant was removed following centrifugation and filtered through a 0.2 μm syringe filter (Ministart®). CFX concentration was determined using UV-Vis HPLC analysis (see SI for details) at 278 nm following calibration with stock CFX solutions.

Determination of Minimum Inhibitory Concentration (MIC)

MICs for all milled samples were measured against *Escherichia coli* ATCC 25922 using broth microdilution technique according to CLSI and EUCAST guidelines. Milled samples were diluted with deionised water in 7 progressive concentrations ranging from 0.064 to 0.001 μg mL^{-1} CFX. Identification of bacterial growth was aided with the addition of resazurin dye, which changes colour in the presence of viable bacteria.

Scanning electron microscopy (SEM). Images of the samples were obtained using an FEI Quanta 600F scanning electron microscope (Oregon, USA). Samples were attached to carbon tabs, mounted on aluminium pins, then sputter-coated with gold for 3 min at 30 mA, using an Emitech K550. Images were recorded under high vacuum, then enhanced using brightness, contrast and astigmatism correction to assess particle size and morphology.

Results and Discussion

CFX Organic Salt Characterization

Powder X-ray Diffraction (PXRD)

Milled products, later identified as ciprofloxacin:succinic acid (CFX-SA), ciprofloxacin:glutaric acid (CFX-GA), ciprofloxacin:adipic acid (CFX-AA) and ciprofloxacin:pimelic acid (CFX-PA), were synthesised by ball milling. PXRD analysis of the milled products indicated formation of novel, crystalline materials. When compared to reference diffraction patterns of the starting materials, novel powder patterns exhibiting sharp diffraction peaks were seen for all four CFX:dicarboxylic acid systems. Notably, diffraction features at low 2θ suggest the presence of large unit cells, as expected for crystalline materials composed of multiple different molecules (Figs. S1 – S4).

Single Crystal X-ray Diffraction (SC-XRD)

Solid phases later identified as CFX-SA, CFX-GA, CFX-AA, CFX-PA CFX-SA hydrate (CFX-SA·H_2O), and CFX-AA hydrate (CFX-AA·H_2O) and were obtained as suitable single crystals by crystallization from aqueous and organic solvents. In each case, proton transfer was confirmed, in line with the agreed understanding of ionization and ΔpK_a in multicomponent crystals.[14] CSD searches showed CFX-SA, CFX-GA, CFX-AA and CFX-PA to be novel crystal structures; the crystal structures of both CFXSA·H_2O and CFXAA·H_2O have previously been reported.[13,28] Whilst the existence of CFX-SA has also been reported,[28] its structure has not. Table 1 summarizes the crystal information for each of the materials and complete, solved structures are included in supplementary information.

CFX-SA crystallizes in space group $P\overline{1}$ with one CFX ion and one SA ion in the asymmetric unit. The positively charged N^+H_2 groups of the piperazinium rings form a centrosymmetric $R_4^4(18)$ motif with the C=O groups of the carboxylates. O5 and O6 of adjacent SA ions are relatively closely spaced at 2.438(2) Å apart; atom H6 lies a somewhat distant 1.09(3) Å from its parent O6, and only 1.35(3) Å through space from O5, leading to interpretation of the structure by OLEX2 as polymeric (Fig. 2; Figs. S5A, S5B; Table S1).

CFX-GA crystallizes in space group $P\overline{1}$ with two CFX ions and two GA ions in the asymmetric unit, with the unique ions in a pseudo-centrosymmetric arrangement. These GA ions form a central $R_2^2(16)$ motif, whilst the positively charged N^+H_2 groups of the piperazinium rings of centrosymmetrically related CFX ions form an $R_4^2(8)$ motif with the carboxylate O^- atoms of two centrosymmetrically related GA ions. In the pseudo-centrosymmetric GA pair: O6 and O12 lie 2.515(1) Å apart, with atom H6 0.95(2) Å from its parent O6 and 1.58 (2) Å through space from O12; O5 and O13 lie 2.502(1) Å apart, with atom H13 0.94(2) Å from its parent O13 and 1.57(2) Å through space from O5. (Figs. S6A, S6B, Table S2)

CFX-AA crystallizes in space group $P2_1/c$ with one CFX ion and one AA ion in the asymmetric unit. Two $D_1^1(2)$ motifs link the positively charged N^+H_2 group of the piperazinium ring to O4 of an AA at *x,y,z* and to O5 of AA at $x,{}^1/_2\text{-}y,{}^-1/_2\text{+}z$. O6 of the AA at *x,y,z* lies 2.508(2) Å from O5 of the AA at $\text{-}1\text{+}x,{}^1/_2\text{-}y,{}^1/_2\text{+}z$, forming a $C_1^1(9)$ motif, with H6 0.93(3) Å from its parent O6 and 1.58(3) Å through space from O5. (Figs. S7A, S7B, Table S3)

CFX-PA crystallizes in space group *Pbca* with one CFX ion and one PA ion in the asymmetric unit. The PA ions form a chain running parallel to the *c* axis, with O5 and O6 of adjacent PA ions are relatively closely spaced at 2.428(1) Å; atom H6 lies a somewhat distant 1.20 (2) Å from its parent O6, and only 1.23(2) Å through space from O5, leading to interpretation of the structure by OLEX2 as polymeric. Two $D_1^1(2)$ motifs link the positively charged N^+H_2 group of the piperazinium ring to O4 of the PA at *x,y,z* and to O5 of the PA at ${}^1/_2\text{-}x,2\text{-}y,{}^-1/_2\text{+}z$. (Figs. S8A, S8B; Table S4).

Comparison of CFX Salts from Milled and Solution Crystallization Methods

That single crystals obtained from solution were representative of the bulk materials obtained by ball milling was confirmed by two approaches. Firstly, single crystals of each of the CFX salts were lightly ground in a mortar and pestle, and the resultant powder subjected to DSC, FT-IR, and PXRD; these characterization methods returned the same results as those obtained from the milled products. Secondly, PXRD data from the bulk materials produced by milling were Pawley fitted in TOPAS,[37] starting from the SC-XRD unit cells. For CFX-GA, CFX-PA and CFX-AA, the unit cell parameters were able to be refined to their room-temperature values and account for all observed diffraction features; for CFX-SA, cell refinement was again successful, leaving only four very weak unaccounted-for diffraction features (Figs. S9 – S12).

Table 1
SC-XRD data for CFX salts generated in this work.

Identification code	CFX-AA	CFX-GA	CFX-PA	CFX-SA
Moiety formula	$(C_{17}H_{19}FN_3O_3)^+$ $(C_6H_9O_4)^-$	$(C_{17}H_{19}FN_3O_3)^+$ $(C_5H_7O_4)^-$	$(C_{17}H_{19}FN_3O_3)^+$ $(C_7H_{11}O_4)^-$	$(C_{17}H_{19}FN_3O_3)^+$ $(C_4H_5O_4)^-$
Formula weight	477.48	463.46	491.51	449.43
Temperature / K	100.00	100.00	100.00	100.00
Crystal system	monoclinic	triclinic	orthorhombic	triclinic
Space group	$P2_1/c$	P-1	$Pbca$	P-1
a / Å	6.94330(10)	7.12370(10)	23.4190(3)	7.2812(3)
b / Å	35.2390(5)	16.3289(2)	8.44410(10)	9.1428(4)
c / Å	9.7722(2)	18.7813(2)	23.5428(3)	16.1257(7)
α / °	90	93.1360(10)	90	75.627(4)
β / °	108.113(2)	99.1070(10)	90	85.627(3)
γ / °	90	91.2250(10)	90	77.389(3)
Volume/Å^3	2272.53(7)	2152.91(5)	4655.64(10)	1014.53(8)
Z	4	4	8	2
ρ_{calc} g/cm^3	1.396	1.430	1.402	1.471
μ/mm^{-1}	0.921	0.955	0.915	0.995
F(000)	1008.0	976.0	2080.0	472.0
Crystal size / mm	0.04 × 0.13 × 0.20	0.05 × 0.06 × 0.15	0.06 × 0.12 × 0.12	0.14 × 0.16 × 0.20
Radiation	Cu Kα	Cu Kα	Cu Kα	Cu Kα
2Θ range for data / °	5.016 to 152.206	4.774 to 157.494	7.51 to 152.38	5.66 to 154.206
Reflections collected	26381	89162	28006	22601
Independent reflections	4611 R_{int} = 0.0486	9172 R_{int} = 0.0707	4724 R_{int} = 0.0294	4089 R_{int} = 0.0669
Data/restraints/parameters	4611/0/323	9172/0/627	4724/0/332	4089/0/308
Goodness-of-fit on F^2	1.064	1.074	1.049	1.070
Final R indexes [I>=2σ (I)]	R_1 = 0.0417 wR_2 = 0.1150	R_1 = 0.0352 wR_2 = 0.0954	R_1 = 0.0324 wR_2 = 0.0827	R_1 = 0.0515 wR_2 = 0.1422
Final R indexes [all data]	R_1 = 0.0456 wR_2 = 0.1189	R_1 = 0.0404 wR_2 = 0.0992	R_1 = 0.0351 wR_2 = 0.0846	R_1 = 0.0600 wR_2 = 0.1487
Largest diff peak/hole /eÅ^{-3}	0.37/-0.30	0.25/-0.25	0.20/-0.23	0.32/-0.38

Fourier-Transform Infrared Spectroscopy (FTIR)

FTIR spectra were taken for CFX salts from milled and solution methods, physical mixtures of the starting materials and CFX HCl·H_2O. CFX salts show differences in stretches compared to reference spectra and physical mixtures, particularly around carboxylic acid carbonyl region (~1700 cm^{-1}) and in the fingerprint region (1500-500 cm^{-1}). This analysis was used to verify salt formation in milled samples in the absence of SC-XRD. Firstly, FTIR spectra of milled materials and crystals obtained from solution were compared and showed identical spectra. FTIR spectra for CFX-SA·H_2O and CFX-AA·H_2O were distinct from those of milled CFX-SA and CFX-AA. The absence of the characteristic ~3200 cm^{-1} signal of -OH bond stretch in bound water suggested that the milled materials do not contain water (Fig. 3). Also seen were differences at the carboxylic acid carbonyl stretch (~1700 cm^{-1}) i.e. a shift from 1720 cm^{-1} to 1700 cm^{-1}. Such changes can be interpreted in terms of different intermolecular bonding as shown in the single-crystal structures.

The reference spectra for CFX base starting material shows a zwitterionic (betaine) form, with ionised carboxylic acid and secondary amine groups. There is an absence of a carboxylic acid carbonyl stretch at ~1700 cm^{-1} and the presence of characteristic asymmetric stretching for carboxylate ion (−COO$^-$) at ~1600 cm^{-1} and ~1400 cm^{-1} (Fig. 4A). FT-IR spectra for CFX-HCl·H_2O confirms this, as a carboxylic acid carbonyl stretch at ~1700 cm^{-1} is present and CFX-HCl·H_2O is known to exist with a neutral carboxylic acid (confirmed experimentally by SC-XRD, Fig. 4B). The FT-IR spectrum for CFX-HCl·H_2O was used as a reference for interpreting bonding in the carbonyl region.

Fig. 5 compares the spectra for CFX-GA with CFX-HCl·H_2O, and GA. For CFX-GA, there are peaks at 1726 cm^{-1} and 1702 cm^{-1} corresponding to neutral carboxylic acid carbonyl stretching in GA and CFX, respectively. The GA peak at 1726 cm^{-1} is also shifted from 1683 cm^{-1} suggesting presence of bonding. There are also strong peaks present in CFX-GA at 1627 cm^{-1} and 1470 cm^{-1}, characteristic of asymmetric stretching for carboxylate ion (−COO$^-$). This mirrors the complex bonding between carboxylic acids seen in SC-XRD data. All milled materials display these characteristic carbonyl peaks confirming formation of salts through milling (Fig. S13 – S16).

Thermal Analysis

DSC analysis showed single sharp endothermic peaks corresponding to crystalline melt for all milled CFX salts, with no exothermic events (Fig. S17 – S20). All CFX salts displayed melting distinct from that of CFX and the corresponding counterion, and all melting points lie between CFX and the counterion melts (Table 2). Melting points increase with molecular weight of coformer, with CFX-PA as an exception; it possesses the lowest melting point of all the four salts. TGA analysis showed no weight loss for any of the milled CFX salts between 30°C and 150°C which confirms the absence of bound water hypothesised from the FT-IR data.

Solubility Measurements

The measured solubilities, starting from each of the CFX salts, are substantially greater than the measured solubility starting from CFX base (Table 3). Interpretation of these solubility measurements is, however, not straightforward. As can be seen, even with 0.2 M phosphate buffer, the pH of the supernatant has shifted away from 6.8 by the end of the 72 hr period. Furthermore, an examination by PXRD of the excess solids recovered at the end of the dissolution experiments shows a complex picture; the excess solids starting from CFX base, CFX-GA, CFX-PA, CFX-SA and CFX-HCl·H_2O all exhibit broadly similar PXRD patterns (Fig. S21) that cannot be explained in terms of the excesses comprising the starting crystalline salt forms being tested. Closer examination, however, reveals some important differences that are apparent in Fig 6, which shows the low angle region of the PXRD patterns. Of particular note is that the excess from the CFX-GA starting material does not exhibit any of the four distinct

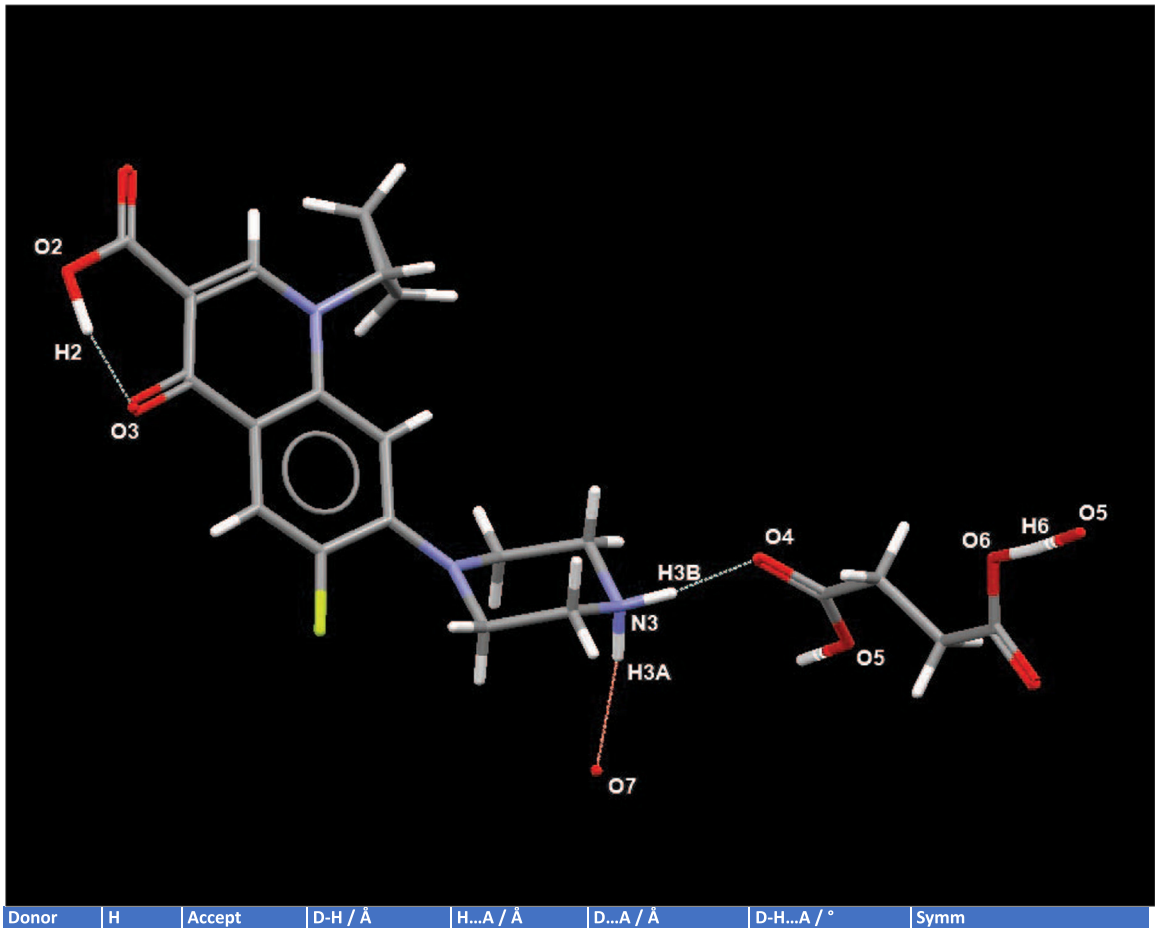

Donor	H	Accept	D-H / Å	H...A / Å	D...A / Å	D-H...A / °	Symm
O2	H2	O3	1.04(4)	1.53(4)	2.545(2)	163(3)	x,y,z
N3	H3A	O7	0.94(3)	1.98(3)	2.8703(19)	157(2)	-x+1,-y+2,-z
N3	H3B	O4	0.92(2)	1.75(2)	2.654(2)	167(2)	x,y,z
O6	H6	O5	1.09(3)	1.35(3)	2.4384(17)	175(2)	x-1,y,z

Fig. 2. A Mercury diagram for the asymmetric unit of CFX-SA, showing the unique set of hydrogen bonds (dashed lines) and the associated bond distances and angles. Note the long O6—H6 bond, which places H6 at a point where it is interpreted as being "shared" with O5, leading to classification of the structure as "polymeric".

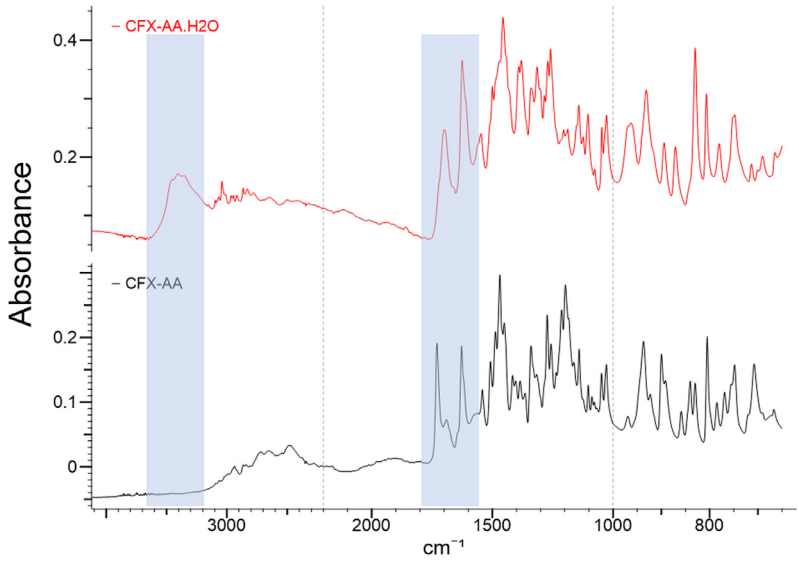

Fig. 3. FTIR spectra of CFX-AA·H_2O (red) and CFX-AA (black) between wavenumbers 600 cm^{-1} and 4000 cm^{-1} with highlighted bound water and carboxylic acid stretching regions. (For interpretation of the references to color in this figure legend, the reader is referred to the web version of this article.)

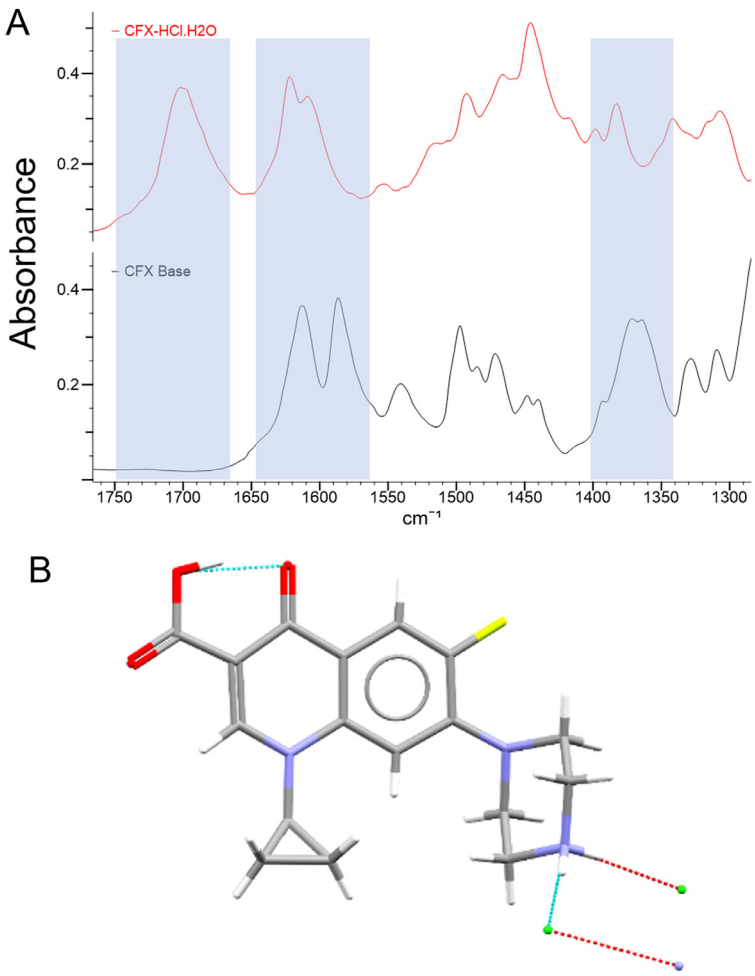

Fig. 4. **(A)** FTIR spectra of CFX-HCl·H_2O (red) and CFX base (black) between wavenumbers 1300 cm^{-1} and 1750 cm^{-1} with highlighted carboxylic acid stretching regions. **(B)** Single-crystal structure of CFX-HCl·H_2O. Ionization of secondary amine and neutral carboxylic acid is seen. (For interpretation of the references to color in this figure legend, the reader is referred to the web version of this article.)

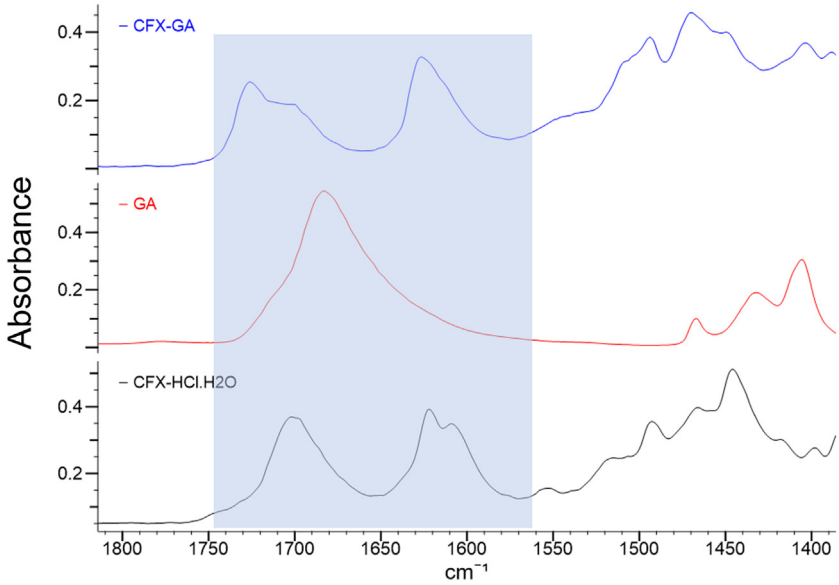

Fig. 5. FTIR spectra of CFX-GA milled (blue) with GA (red) and CFX-HCl·H_2O references (black) between wavenumbers 1350 cm^{-1} and 1800 cm^{-1} with highlighted carboxylic acid stretching regions. (For interpretation of the references to color in this figure legend, the reader is referred to the web version of this article.)

Table 2
DSC data for CFX and CFX salts compared to counterion MWt and MPt.

	MP (°C)	Counterion MWt (g.mol^{-1})	Counterion MPt (°C)
CFX base	273.24	n/a	n/a
CFX-SA	218.44	118.09	192.08
CFX-GA	222.05	132.12	99.63 (75.58)
CFX-AA	234.53	146.14	154.50
CFX-PA	191.25	160.17	107.38

peaks in the range 6-8° 2θ shown by CFX base, CFX-PA, CFX-SA and CFX-HCl·H_2O, whilst the excess of the CFX-Base starting material does not exhibit the peak at ca. 11.5° 2θ that is shared by the excesses from all of the other starting salt forms shown. It is thus likely that the excesses consist of phase mixtures, and that the composition of the excess starting from CFX-GA is markedly different from that of the others, this latter observation being the cause of its higher observed solubility. We have not as yet been successful in explaining the observed PXRD data for these excesses in terms of reported forms of CFX, its salts and its hydrates. However, in the case of the excess solid from the CFX-AA starting material experiment, which gives rise to a significantly different PXRD pattern (Fig. S22) from the other starting materials, we conclude that it is largely composed of ciprofloxacin hemikis(adipate) dihydrate [CSD refcode QUKHOV] (Fig. S23). This conclusion is supported by the fact that a small single crystal, whose experimental cell dimensions matched those of QUKHOV, was retrieved from the excess, and by the strong level of agreement between the observed PXRD data and a calculated PXRD pattern for QUKHOV.

Overall, it is unclear exactly what physical forms the saturation solubility values determined in the work pertain to. Nevertheless, it is noteworthy that CFX-GA, whose solid excess does not match those of the other salts, does give rise to the highest solubility of any of the salts examined.

Minimum Inhibitory Concentration (MIC)

Following incubation, plates were analysed to determine lowest concentration of ciprofloxacin salt which completely inhibited *E. coli* growth. All CFX salts showed an MIC within the acceptable range for CFX-HCl·H_2O as validated by EUCAST (i.e. Target = 0.008 g/L; Range = 0.004 g/L to 0.016 g/L) (Fig. S24). CFX-SA, CFX-GA and CFX-AA showed MIC of 0.008 g/L and CFX-PA showed MIC of 0.004 g/L.

Table 3
Solubility measurements for CFX base, CFX-HCl·H2O, and the salt forms generated in this work.

	0.1 M Phosphate Buffer pH 6.8		0.2 M Phosphate Buffer pH 6.8	
Formulation	Final pH	Solubility (mg mL^{-1})	Final pH	Solubility (mg mL^{-1})
CFX Base	-	0.04	6.93	1.20
CFX-HCl·H_2O	-	14.36	5.20	5.55
CFX-SA	5.32	8.43	5.64	5.81
CFX-GA	5.22	107.83	5.43	13.55
CFX-AA	5.62	4.28	5.61	4.02
CFX-PA	5.61	13.79	5.90	5.15

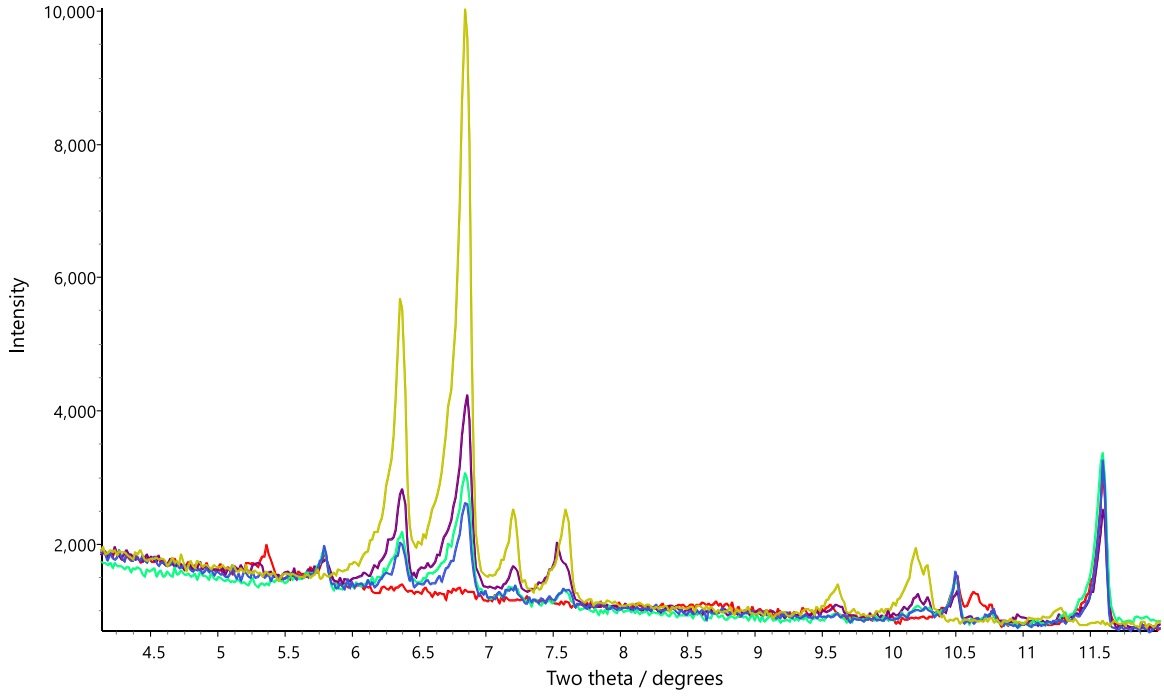

Fig. 6. The low-angle region of PXRD patterns for excess solids recovered at the end of the dissolution experiments. Starting materials: CFX-GA (red), CFX-SA (green), CFX-PA (purple), CFX-Base (mustard) and CFX-HCl·H_2O (blue). (For interpretation of the references to color in this figure legend, the reader is referred to the web version of this article.)

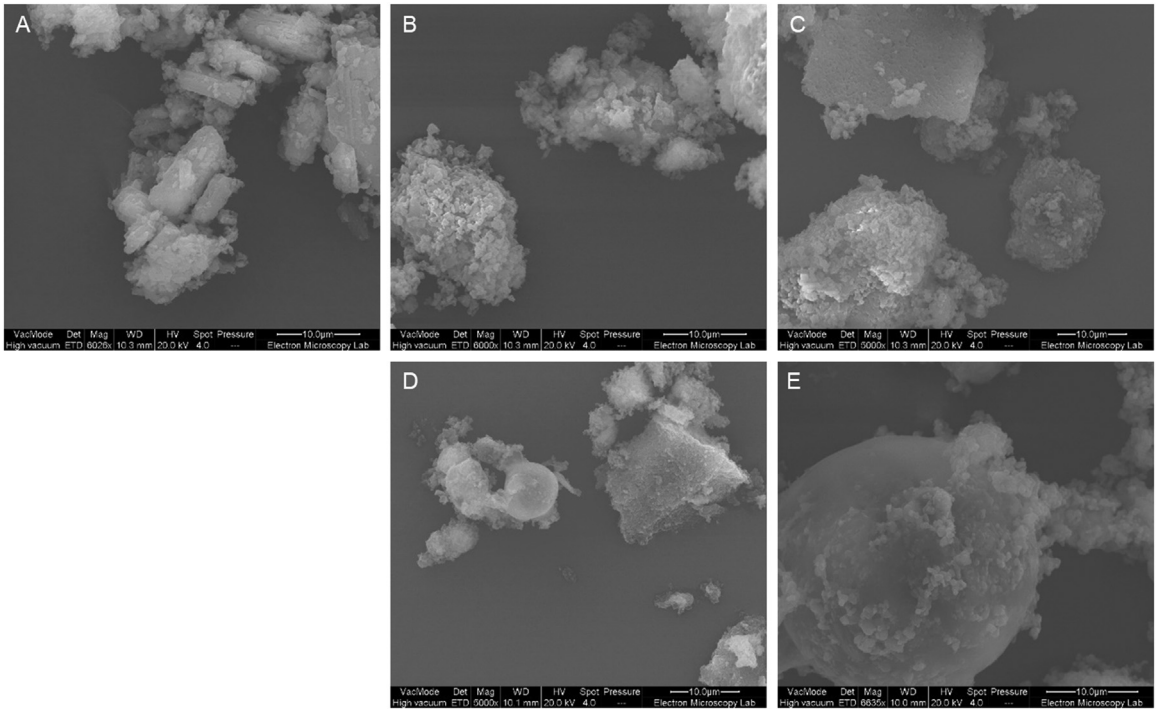

Fig. 7. SEM images for CFX base (A) compared to CFX-SA (B), CFX-GA (C), CFX-AA (D), CFX-PA (E) milled salts. Milled CFX salts appear to have lost needle crystal habit of CFX base and show some signs of agglomeration. Approximate particles size appears to be greater than 10 μm, although irregular shapes exist.

CFX salts did not show a detrimental impact on antibacterial activity showing equivalent results to CFX-HCl·H_2O. This confirms that in this case, physicochemical property change does not alter antimicrobial activity.

Scanning Electron Microscopy (SEM)

SEM micrographs of milled CFX salts are shown in Fig. 7. The powders showed a wide range of particle sizes and surface morphologies. The semi-regular "needle like" crystal habit of CFX base has been removed by ball milling. Furthermore, CFX salt particles appear more aggregated than CFX base raw material, which is common for ball milled powders. It is well known that reduced average particle size can be advantageous for a variety of pharmaceutical physicochemical properties e.g. dissolution and aerodynamic properties.[38,39] SEM images showed the presence of some large (> 10 μm) particles and as such, the next stage in formulation development for these CFX salts would most likely need to consider particle size reduction and control.

Conclusion

Crystalline CFX salts with distinct physicochemical properties have been successfully produced by ball milling and solution crystallization. Proton transfer between CFX and acid counterions was confirmed through SC-XRD and FTIR analysis. Melting point analysis showed single crystalline melts located between CFX and corresponding acids. However, neither counterion molecular weight nor melting point seem to have an influence on observed melting points. Saturation solubility experiments, coupled with PXRD analysis of excess solids, reveal a complex picture of phase transformations and a CFX-GA salt form that results in a markedly higher solubility than that of CFX-HCl·H_2O. Antibacterial activity of all the novel salt forms against free bacteria has been confirmed. The existence of novel solid forms of CFX may help extend its pharmaceutical use beyond that of the traditional oral formulation with CFX-HCl·H_2O. Further studies to assess the key properties of these CFX salts are required, especially focusing on explaining physical form transformations in solution and observing counterion activity against bacterial biofilms.

Funding Sources

This work was supported by Quotient Sciences and the Engineering and Physical Sciences Research Council (EPSRC UK) [grant number 2266759].

Conflict of Interest Disclosure

The authors declare no conflict of interest.

Acknowledgments

The authors would like to thank the Chemical Analysis Facility (CAF) at the University of Reading for providing essential access to instruments used in this study. We are grateful to the UK Materials & Molecular Modelling Hub for computational resources, which is partially funded by EPSRC (EP/P020194/1 and EP/T022213/1), for DFT-D calculations used to verify H atom locations in the CFX salts. We are also grateful to Dr. Norman Shankland, for useful discussions on solubility measurements and the PXRD data obtained from the excess solids.

Supplementary Materials

Supplementary material associated with this article can be found, in the online version, at doi:10.1016/j.xphs.2022.08.008.

References

1. Sathisaran I, Dalvi SV. Engineering cocrystals of poorlywater-soluble drugs to enhance dissolution in aqueous medium. *Pharmaceutics*. 2018;10(3):108.

2. Williams H, Trevaskis N, Charman S, et al. Strategies to address low drug solubility in discovery and development. *Pharmacol Rev*. 2013;65:315–499.
3. Shi Q, Moinuddin SM, Cai T. Advances in coamorphous drug delivery systems. *Acta Pharm Sinica B*. 2019;9(1):19–35.
4. Blagden N, de Matas M, Gavan PT, York P. 2007. Crystal engineering of active pharmaceutical ingredients to improve solubility and dissolution rates. ed. p 617-630.
5. Duggirala NK, Perry ML, Almarsson Ö, Zaworotko MJ. Pharmaceutical cocrystals: along the path to improved medicines. *Chem Commun*. 2016;52(4):640–655.
6. Al-Obaidi H, Majumder M, Bari F. Amorphous and crystalline particulates: challenges and perspectives in drug delivery. *Curr Pharm Des*. 2017;23(3):350–361.
7. Al-Obaidi H, Lawrence MJ, Buckton G. Atypical effects of incorporated surfactants on stability and dissolution properties of amorphous polymeric dispersions. *J Pharm Pharmacol*. 2016;68(11):1373–1383.
8. Xiong X, Du Q, Zeng X, He J, Yang H, Li H. Solvates and polymorphs of rebamipide: preparation, characterization, and physicochemical analysis †. *RSC Adv*. 2017;7:23279–23286.
9. Hu Y, Gniado K, Erxleben A, McArdle P. Mechanochemical reaction of sulfathiazole with carboxylic acids: formation of a cocrystal, a salt, and coamorphous solids. *Cryst Growth Des*. 2014;14(2):803–813.
10. Al-Obaidi H, Kowalczyk RM, Kalgudi R, Zariwala MG. Griseofulvin solvate solid dispersions with synergistic effect against fungal biofilms. *Colloids Surf B*. 2019;184:110540.
11. McShane PJ, Weers JG, Tarara TE, et al. *Ciprofloxacin Dry Powder for Inhalation (Ciprofloxacin DPI): Technical Design and Features of an Efficient Drug–Device Combination*. Academic Press; 2018:72–79.
12. Florindo C, Costa A, Matos C, et al. Novel organic salts based on fluoroquinolone drugs: Synthesis, bioavailability and toxicological profiles. *Int J Pharm*. 2014;469(1):179–189.
13. Surov AO, Manin AN, Voronin AP, et al. Pharmaceutical salts of ciprofloxacin with dicarboxylic acids. *Eur J Pharm Sci*. 2015;77:112–121.
14. Gunnam A, Suresh K, Ganduri R, Nangia A. Crystal engineering of a zwitterionic drug to neutral cocrystals: a general solution for floxacins. *Chem Commun*. 2016;52:12610–12613.
15. Basavoju S, Boström D, Velaga SP. Pharmaceutical cocrystal and salts of norfloxacin. *Cryst Growth Des*. 2006;6(12):2699–2708.
16. de Almeida AC, Torquetti C, Ferreira PO, et al. Cocrystals of ciprofloxacin with nicotinic and isonicotinic acids: Mechanochemical synthesis, characterization, thermal and solubility study. *Thermochim Acta*. 2020;685: 178346.
17. Chen X, Partheniadis I, Nikolakakis I, Al-Obaidi H. Solubility improvement of progesterone from solid dispersions prepared by solvent evaporation and co-milling. *Polymers*. 2020;12(4):854.
18. Uhljar LE, Kan SY, Radacsi N, Koutsos V, Szabo-Revesz P, Ambrus R. In vitro drug release, permeability, and structural test of ciprofloxacin-loaded nanofibers. *Pharmaceutics*. 2021;13(4).
19. Mesallati H, Conroy D, Hudson S, Tajber L. Preparation and characterization of amorphous ciprofloxacin-amino acid salts. *Eur J Pharm Biopharm*. 2017;121:73–89.
20. Olivera ME, Manzo RH, Junginger HE, et al. Biowaiver monographs for immediate release solid oral dosage forms: ciprofloxacin hydrochloride. *J Pharm Sci*. 2011;100(1):22–33.
21. Mohammed A, Zurek J, Madueke S, et al. Generation of high dose inhalable effervescent dispersions against pseudomonas aeruginosa biofilms. *Pharm Res*. 2020;37(8):150.
22. Paulekuhn GS, Dressman JB, Saal C. Trends in active pharmaceutical ingredient salt selection based on analysis of the orange book database. *J Med Chem*. 2007;50(26):6665–6672.
23. Kawabata Y, Wada K, Nakatani M, Yamada S, Onoue S. *Formulation Design for Poorly Water-Soluble Drugs Based on Biopharmaceutics Classification System: Basic Approaches and Practical Applications*. Elsevier B.V; 2011:1–10.
24. Berge SM, Bighley LD, Monkhouse DC. Pharmaceutical salts. *J Pharm Sci*. 1977;66(1):1–19.
25. Carvalho Jr P, Diniz L, Tenorio J, et al. 2019. Pharmaceutical paroxetine-based organic salts of carboxylic acids with optimized properties: the identification and characterization of potential novel API solid forms. 21:3668−3678.
26. Bahamondez-Canas T, Smyth HDC. Influence of excipients on the antimicrobial activity of tobramycin against pseudomonas aeruginosa biofilms. *Pharm Res*. 2018;35(1):10.
27. Dayo Owoyemi BC, Da Silva CCP, Souza MS, Diniz LF, Ellena J, Carneiro RL. Fluconazole: synthesis and structural characterization of four new pharmaceutical cocrystal forms. *Cryst Growth Des*. 2019;19(2):648–657.
28. Paluch KJ, McCabe T, Müller-Bunz H, Corrigan OI, Healy AM, Tajber L. Formation and physicochemical properties of crystalline and amorphous salts with different stoichiometries formed between ciprofloxacin and succinic acid. *Mol Pharmaceutics*. 2013;10(10):3640–3654.
29. Fábián L. Cambridge structural database analysis of molecular complementarity in cocrystals. *Cryst Growth Des*. 2009;9(3):1436–1443.
30. Childs SL, Stahly GP, Park A. The salt−cocrystal continuum: the influence of crystal structure on ionization state. *Mol Pharmaceutics*. 2007;4(3):323–338.
31. Lu J, Rohani S. Preparation and characterization of theophylline−nicotinamide cocrystal. *Org Process Res Dev*. 2009;13(6):1269–1275.
32. Sheldrick G. SHELXT - Integrated space-group and crystal-structure determination. *Acta Crystallogr, Sect A*. 2015;71(1):3–8.
33. Sheldrick G. Crystal structure refinement with SHELXL. *Acta Crystallogr Section C*. 2015;71(1):3–8.
34. Dolomanov OV, Bourhis LJ, Gildea RJ, Howard JAK, Puschmann H. OLEX2: a complete structure solution, refinement and analysis program. *J Appl Crystallogr*. 2009;42(2):339–341.
35. Groom CR, Bruno IJ, Lightfoot MP, Ward SC. The Cambridge structural database. *Acta Crystallogr Section B*. 2016;72(2):171–179.
36. Macrae CF, Sovago I, Cottrell SJ, et al. Mercury 4.0: from visualization to analysis, design and prediction. *J Appl Crystallogr*. 2020;53(1):226–235.
37. Coelho AA. TOPAS and TOPAS-Academic: an optimization program integrating computer algebra and crystallographic objects written in C++. *J Appl Crystallogr*. 2018;51(1):210–218.
38. Savjani KT, Gajjar AK, Savjani JK. Drug solubility: importance and enhancement techniques. *ISRN Pharmaceutics*. 2012;2012:1–10.
39. Chow AHL, Tong HHY, Chattopadhyay P, Shekunov BY. *Particle Engineering for Pulmonary Drug Delivery*. 20072007:411–437.